AN EXPERIMENTAL INVESTIGATION OF THE OBLIQUE BLADE-VORTEX INTERACTION

M.B. Horner, E. Saliveros, R.A.McD. Galbraith
University of Glasgow
Glasgow, Scotland

Abstract

The experimental results of an oblique Blade-Vortex Interaction (BVI) study are presented. The quality of all pressure data reflects improvements in the Glasgow University BVI facility and in the method of reducing and presenting data. The data collected during oblique interactions is found qualitatively and quantitatively similar to that collected in corresponding parallel interactions, for interactions within $\pm$ 30° of parallel. Details of the pressure data are examined in the light of understanding gained from parallel BVI experimentation. The study highlights the effects of three dimensional flow interactions not accounted for in the nondimensionalisation traditionally utilised in the analysis of parallel blade-vortex interactions.

Nomenclature

c	blade chord length
C_{mQC}	quarter chord moment coefficient
C_n	normal force coefficient
C_p	pressure coefficient
C_t	tangential force coefficient
r	radial position of pressure measurement pod
R	blade radius
R_e	Reynolds number
t	time
V_x	chordwise velocity at the measurement position when $X_v/c=0.5$
X_v	horizontal distance between the leading edge pressure transducer and the vortex centre, measured perpendicular to the vortex core
Y_v	vertical displacement of the vortex generator junction above the rotor disk
Z_v	lateral displacement of the vortex generator from the tunnel centreline
Γ	vortex circulation
$\bar{\Gamma}$	nondimensional vortex circulation ($\bar{\Gamma} = \Gamma/(cVx)$)
Ω	angular velocity of the rotor blade
Ψ	blade azimuth angle

Introduction

Under certain conditions of powered descent or vigorous manoeuvring, rotorcraft blades pass through the wake and trailed tip vortices from previous blades (see Fig. 1). This interaction of the rotor blade with the tip vortex of a preceding blade is a significant source of noise and vibration in rotorcraft[1]. The need to reduce these undesirable effects requires that the rotorcraft designer has a clear understanding of the fluid dynamics underlying the
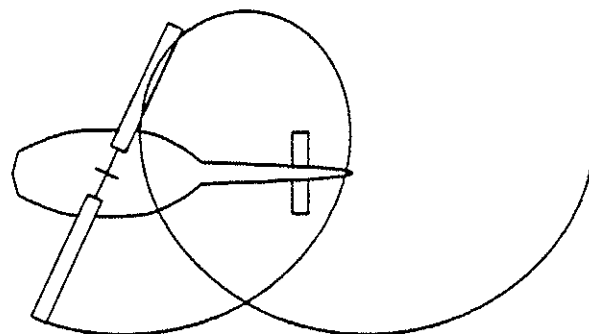

Fig. 1: Schematic of blade-vortex interaction during rotorcraft flight.

phenomena of blade-vortex interaction. This need has been addressed through both experimental[1-15] and computational[16-18] studies attempting to isolate the BVI from the rotor environment.

While many of these BVI studies confine themselves to two-dimensional[8-12,15,18-20] or steady-state[8] examinations of the blade-vortex interaction, few have gone on to consider the added complexity of the oblique BVI[2,3,5,6]. Both the Surendraiah[2]/Padakannaya[3] experiment and the experiment of Caradonna et al[5] isolated the oblique BVI in wind tunnel tests involving an upwind vortex generating wing tip and a downwind rotor. The oblique angle of interaction was controlled by adjusting the spanwise distance between the vortex generator and the rotor hub. The Surendraiah/Padakannaya experiment exhibited great ingenuity in pioneering this approach, but suffered from a scarcity of pressure transducers and automatic data processing, thus weakening the resolution of C_p and C_n data, and unfortunately rendering C_m and C_t data virtually unobtainable. Caradonna et al presented a limited test matrix, and only in C_p form, leaving many of the interesting facets of the integrated force coefficients unexplored.

The Glasgow University BVI facility isolates the BVI in a manner similar to that used by Surendraiah, Padakannaya and Caradonna et al. The quality of data collected with Glasgow's improved system has allowed a thorough investigation of many facets of the oblique BVI. In addition, the large test matrix, incorporating many different parallel and oblique geometries, has permitted a close comparison of oblique and parallel BVI data, thus highlighting the effects of three-dimensional test conditions.

Methods

Experiments were conducted in the University of Glasgow "Handley Page" wind tunnel. An untwisted, non-lifting, single blade rotor interacted in a parallel or oblique mode with an oncoming vortex generated upstream of the rotor disk by a stationary wing. This set-up is depicted in Fig. 2.

The rotor blade has a NACA 0015 aerofoil section, with a 0.149m chord and a 0.9426m radius. An instrumented pod containing 26 miniature pressure transducers (3 KULITE XCS-093-5-SG transducers and 23 ENTRAN-EPIL-080B-5S transducers) could be fit into the blade at one of 5 spanwise positions. The 26 transducer voltages were amplified, low pass filtered, then simultaneously
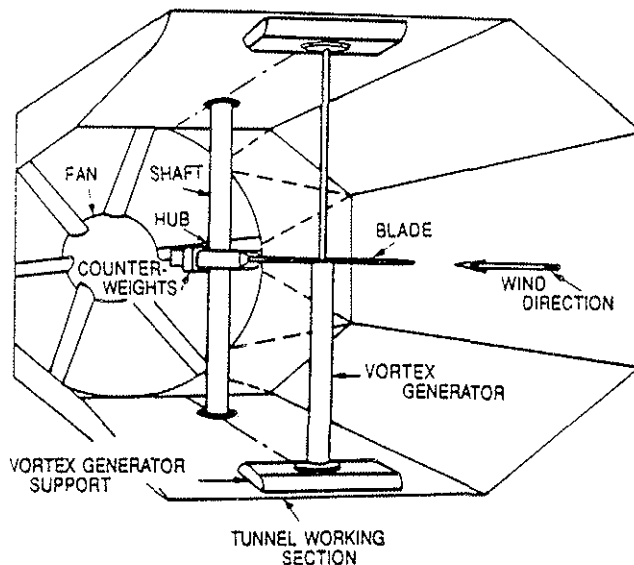

Fig. 2: The new Glasgow University BVI facility in the Handley Page wind tunnel.

digitised by a Thorn EMI BE256-420 data logger, before being stored in an IBM PS/2 80/041 computer for further reduction and presentation. Data collection was phase locked to azimuth position, and each test run comprised the collection of data during many (typically 7) interactions. Data were subsequently ensemble averaged about the C_n cross over point, the point near $X_v/c = 0.0$, where the normal force drops through zero, between the peak and the nadir in C_n.

The vortex generator was made up of two adjoining NACA 0015 aerofoil sections spanning the height of the test section 2.1 rotor radii upstream of the rotor hub. The vortex strength was controlled by setting the two sections at equal but opposite incidence. The magnitudes of the vortex strength were identical to those used by Kokkalis and Galbraith[13,14], who measured vortex circulation by means of a triple hot-wire probe. The horizontal position of the vortex generator (Z_v) determined the angle of intersection between the interaction vortex and the blade, resulting in either a parallel or oblique BVI. The vertical position of the aerofoil junction on the vortex generator (Y_v) was altered to vary the height of the interaction vortex above the rotor disk. The full test matrix is presented in Table 1.

For tests the rotor and vortex generator were situated together in the 1.61 x 2.13m octagonal test section. The tunnel was run at 47.0 m/s, while the rotor was rotated with a tip speed of 59.3 m/s. The comparable aerodynamic scaling of the vortex generator and the rotor assured a realistically scaled BVI.

	$r/R =$ 0.944	$r/R =$ 0.865	$r/R =$ 0.785	$r/R =$ 0.706	$r/R =$ 0.626
$Z_v/c = 2$	$\Gamma = 0.630$	$\Gamma = 0.660$	$\Gamma = 0.691$	$\Gamma = 0.718$	$\Gamma = 0.743$
$Z_v/c = 1$	$\Gamma = 0.707$	$\Gamma = 0.754$	$\Gamma = 0.806$	$\Gamma = 0.863$	$\Gamma = 0.923$
$Z_v/c = 0$ (parallel)	$\Gamma = 0.804$ 0.612 0.408 0.264 0.132	$\Gamma = 0.878$ 0.668 0.446 0.288 0.144	$\Gamma = 0.967$ 0.736 0.491 0.318 0.159	$\Gamma = 1.076$ 0.819 0.546 0.353 0.177	$\Gamma = 1.213$ 0.923 0.615 0.398 0.199
$Z_v/c = -1$	$\Gamma = 0.936$	$\Gamma = 1.055$	$\Gamma = 1.214$	$\Gamma = 1.438$	$\Gamma = 1.784$
$Z_v/c = -2$	$\Gamma = 1.110$	$\Gamma = 1.319$	$\Gamma = 1.620$	$\Gamma = 2.147$	$\Gamma = 3.293$

Table 1. A test matrix of blade-vortex interactions examined. All cases were tested at eleven values of vortex aerofoil separation height: Y_v/c = 1.0, 0.8, 0.6, 0.4, 0.2, 0.0, -0.2, -0.4, -0.6, -0.8, -1.0.

Pressure data were integrated around the aerofoil section to provide force and moment data. Pressure, force and moment data were nondimensionalised into aerodynamic coefficients using the local chordwise velocity at the measurement location when X_v/c = 0.5. The nondimensional time variable, X_v/c was computed from the geometry of the blade and does not account for BVI induced perturbations to the vortex position. More detail on the experimental set-up and procedure may be found in Homer et al[16].

Results

During tests, pressure data were collected at 26 locations around the chord of a test aerofoil during oblique interaction with a free vortex. The pressure and integrated force data showed many of the same features observed by other researchers in parallel BVI studies. Pressure data were dominated by the build up of the leading edge suction peak during the approach of the interacting vortex, while normal force data were characterised by the build up and then sudden reversal of C_n. Pressure and normal forces also showed variations in magnitude and alterations in form due to the three dimensional flows resulting from the oblique interactions.

An example of typical averaged data from an oblique BVI is presented in Fig. 3. In this test the vortex generator was offset 0.98 chord lengths from the tunnel centreline, to produce a second quadrant oblique BVI that

was 10.3° from parallel. The nondimensional vortex strength was 0.754, the vortex passed 0.2 chord lengths above the blade, and the measurement pod was positioned at the 86.5% span location. The surface plot portrays the evolution of the pressure acting on the upper surface during the BVI. The surface plot is made up of a stacked sequence of chordwise pressure distributions. The first pressure distribution, representing data taken at X_v/c = -2.269, is in the foreground. This pressure distribution is shaped in a manner consistent with the suction side of an aerofoil, reflecting the increasing incidence produced by the approaching vortex. Subsequent pressure distributions, stacked in sequence towards the rear, show the growth of the leading edge suction peak, which reaches a maximum just before the vortex passes the leading edge near X_v/c = 0.0. The dramatic collapse of the suction peak at this point is followed by a jagged ridge that slants away towards the trailing edge as the interaction continues. This ridge marks a "convective disturbance" that has been associated with the overhead passage of the vortex[5,17]. The jagged appearance of this ridge reflects the influence of the disturbance on the consecutive discrete transducer locations. After this disturbance convects off of the aerofoil upper surface near $X_v/c = 0.8$, the pressure distributions take on the character of the pressure side of an aerofoil at low incidence.

To the right of the surface plot in Fig. 3 are three plots presenting the integrated force and moment histories derived from the pressure data for this BVI. The C_n data reflects the initial increase in angle of attack as the vortex approaches the leading edge, and the sudden reversal of lift as the vortex passes the leading edge, reversing the angle of attack and collapsing the suction peak evident in the C_p surface plot. The ensuing negative lift is somewhat suppressed by the low pressure region of the vortex pulling on the upper surface, but as the vortex passes the trailing edge the data show a momentary downward spike as the aerofoil regains the negative lift lost to the suction of the vortex on the upper surface. This momentary spike in negative lift is further enhanced by a brief trailing edge suction pulse that appears on the lower surface as the vortex passes the trailing edge. The C_n spike has been correlated with the trailing edge passage of the vortex in parallel BVI investigations[17,20].

The C_{mQC} history also highlights the effect of the convecting vortex on the aerofoil pressure distribution. The initial increase in moment reflects the disparity in vortex induced angle of attack between the leading and trailing edges. As the vortex passes over the chord the low pressure associated with the vortex dominates the

moment, initially producing a peak in the pitch up moment, and then, as the vortex moves aft, pulling up on the trailing edge to induce a strong pitch down moment. The data then show a sharp positive spike to the maximum C_{mQC} as the vortex leaves the trailing edge, replacing the upper surface trailing edge suction (associated with the vortex) with a higher pressure associated with the strong downwash of the aft convecting vortex. This high spike is also enhanced by the suction pulse that the vortex raises at the trailing edge of the lower surface at this time. The moment spike drops back below zero as this suction pulse disappears, and the moment then converges back towards zero as the vortex convects downstream, reducing the aerofoil incidence towards a more uniform value of zero.

The tangential force coefficient history is dominated by the large forward force generated by the approaching vortex. This force peaks as the low pressure vortex arrives at the leading edge of the aerofoil, and then abruptly reverses as the vortex passes the leading edge. The significance of the second minimum in tangential force is not at this time understood.

The prominence of the ridge in C_p associated with the convecting vortex, and the type of perturbations to the the integrated coefficient histories resulting from trailing edge vortex effects are strongly dependent upon the direction and magnitude of the vortex height (Y_v). In all cases examined however, the effects of the overhead passage of the vortex during oblique interactions was similar to the effects observed during corresponding parallel interactions by Horner et al[17].

Figure 4 presents a comparison of the integrated force and moment data measured under parallel and oblique conditions. All three tests were run with a vortex strength (Γ) of 6.7 m^2/s, a vortex height (Y_v) of 0.2c, and with the measurement pod at the 86.5% span location. The lateral displacement of the vortex generator, however, was different in each of these tests. In the data curves embedded with the round symbols, the vortex generator was set 2 chord lengths to the positive Z_v side of the tunnel centreline, resulting in an oblique BVI in the second quadrant. Because the rotor blade is moving into the wind in this quadrant, the relative wind

B.V.I. "OBLIQUE" TEST	RUN REFERENCE NUMBER : B8511

Blade Section: " NACA - 0015 "
Spanwise Position r/R = 0.865
Vortex Separation, Yv/C = 0.200
Zv/C = 0.980

Vortex Strength, Γ = 6.70 m^2/s
Tip Reynolds Number, Re = 600000
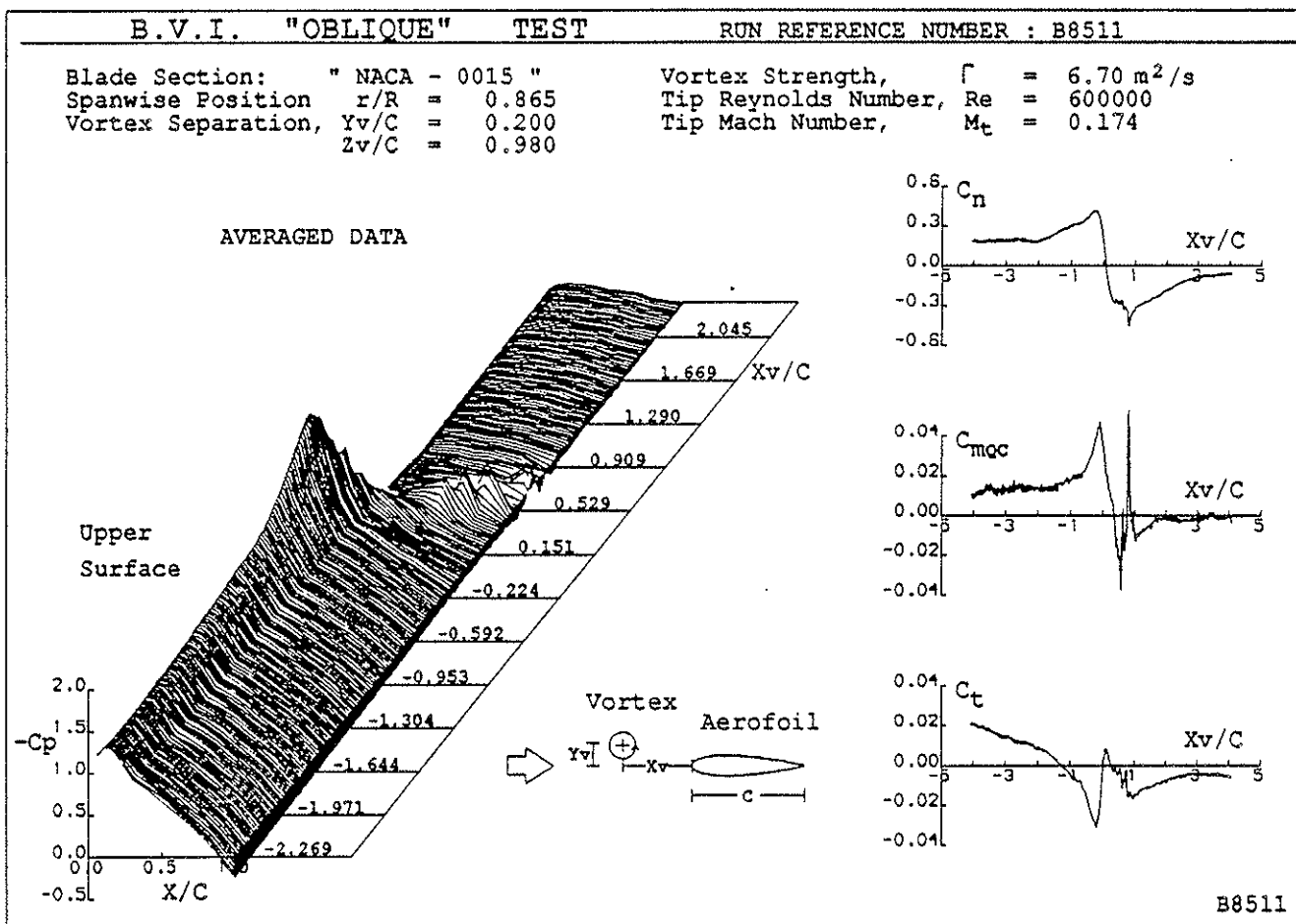Tip Mach Number, M_t = 0.174

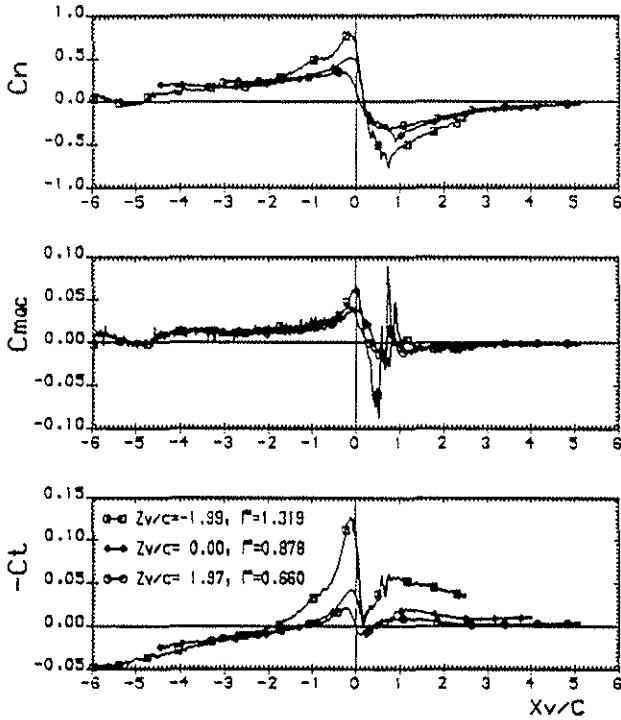Fig. 3: Typical data from an oblique blade-vortex interaction.

Fig. 4: A comparison of integrated force and moment data from parallel and oblique blade-vortex interactions. All cases measured at r/R = 0.865, with Y_v/c = 0.2, Γ = 6.7m^2/s.

impinging upon the measurement position is greater than during purely parallel tests, resulting in a reduction of the relative vortex influence, and a corresponding reduction in the nondimensional vortex strength. $\bar{\Gamma}$ was 0.660 in this case. The curves embedded with the diamond symbols represent data taken with the vortex generator aligned with the rotor hub on the tunnel centreline, resulting in a parallel BVI with $\bar{\Gamma}$ = 0.878. The data curves with the square symbols reflect data taken with the vortex generator set 2 chord lengths to the negative Z_v side of the tunnel centreline, resulting in a third quadrant oblique BVI. In the third quadrant, the relative wind impinging upon the measurement position is less than under parallel conditions, enhancing the relative influence of the interaction vortex, and resulting in the large nondimensional vortex strength of 1.319.

The gross features of the C_n, C_m, and C_t curves in Fig. 4 are similar to those exhibited by the integrated force and moment curves in Fig. 3. The C_n curves in Fig. 4 show the same rise to a peak, followed by a reversal of lift, that was tied to the growth and collapse of the suction peak in Fig. 3. Each of the C_n curves in Fig. 4 shows a negative spike corresponding to the C_n spike associated with vortex-trailing edge passage in Fig. 3.

The moment histories in Fig. 4 also show a good degree of qualitative agreement with the C_m curve in Fig. 3, presumably reflecting similar vortex influences associated with the vortex height of 0.2c. And finally the C_t curves in Fig. 4 show the same early peak that was tied to the approach of the vortex in Fig 3, and the same secondary peak which fades as the vortex convects downstream.

Although the data sets presented in Fig. 4 show many similarities in their gross features, it is the large differences in magnitude that are most striking. The variation in magnitude of the peaks, valleys, and perturbations in these curves corresponds to the variations in the nondimensional vortex strength, which is tied to changes in relative wind in the different quadrants examined. The large scale of these variations obscures the more subtle influences of variation in Z_v, the parameter controlling the blade-vortex intersection angle.

By varying other parameters simultaneously with Z_v, comparisons can be made between parallel and oblique interactions with similar nondimensional vortex strengths.

Fig. 5 presents a comparison of integrated force and moment data from parallel and second quadrant oblique interactions with similar nondimensional vortex strengths. Both data sets were measured at the 86.5% span location, in both cases Y_v was set to 0.2c. The same second quadrant oblique BVI is examined in Fig. 5 as was examined in Fig. 4, the nondimensional vortex strength in this case is 0.660. The parallel BVI data was measured using a weaker vortex (Γ = 5.1 m^2/s) than in Fig. 4, resulting in a nondimensional vortex strength of 0.668.

The gross features of the curves in Fig. 5 are similar to those observed in the data curves of Figures 3 and 4. More subtle differences between the curves of Fig. 5 highlight the differences between parallel and second quadrant oblique interactions. In the upper plot, a comparison of the normal force histories reveals that in the early stages the oblique interaction has larger C_n values. Subsequently the oblique case C_n values climb more slowly than in the parallel case, have a lower and more rounded peak and drop towards a negative value slightly less steeply than in the parallel case. After the interaction vortex has passed the leading edge the two curves show rapid convergence, and are almost indistinguishable as the vortex convects past the aerofoil upper surface and into the wake. The C_m and C_t curves
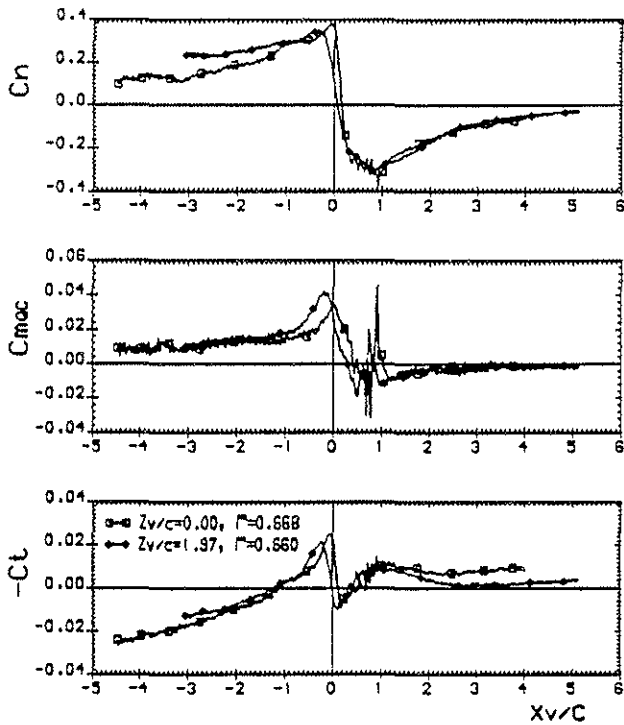
487

Fig. 5: A comparison of integrated force and moment data from comparable parallel and 2nd quadrant oblique interactions. Both cases measured at r/R = 0.865, with Y_v/c = 0.2. Γ = 6.7m²/s during oblique test, Γ = 5.1 m²/s during parallel test.
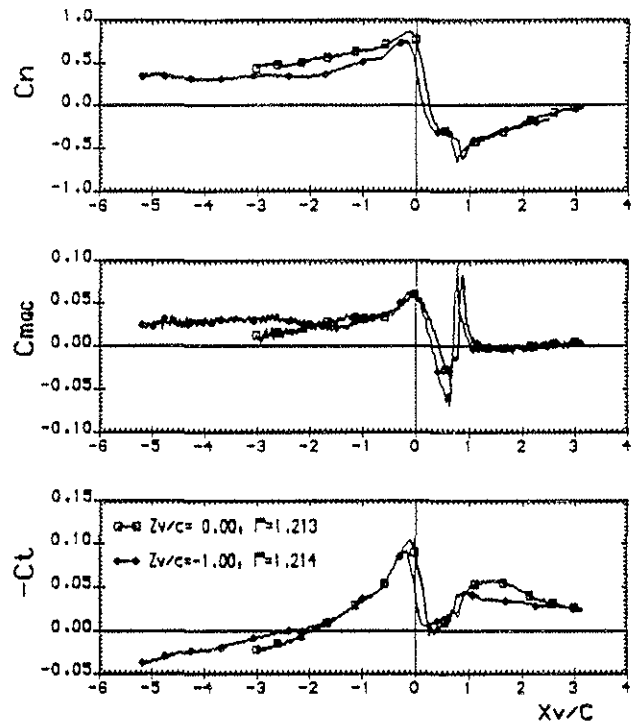
Fig. 6: A comparison of integrated force and moment data from comparable parallel and 3rd quadrant oblique interactions. Both cases measured with Y_v/c = 0.2, Γ = 6.7 m²/s. r/R = 0.785 during oblique test, r/R = 0.626 during parallel test.

show a similar response to the final approach of the vortex, with the coefficients showing a more rounded peak under oblique interaction conditions than under parallel conditions. In the case of C_m this peak is higher in the oblique test, but in the C_t plot, as in the C_n plot, the parallel test produces the highest peak.

The previously noted variations between data collected under parallel and oblique conditions are typical of all comparisons made, using the present data, between similarly scaled parallel and second quadrant oblique interactions. The slight phase shift between peaks in Fig. 5, and between trailing edge moment perturbations, is not universal in such comparisons. Neither is the difference in the magnitudes of the trailing edge moment perturbations evident in Fig.5.

A comparison of a third quadrant oblique BVI with a parallel BVI of a similar nondimensional vortex strength is shown in Fig. 6. The parallel BVI was measured at the 62.6% span location, while Y_v=0.2c, Γ=6.7 m²/s, and $\overline{\Gamma}$ = 1.213. During the third quadrant oblique BVI, data was measured at the 78.5% span location, while

Y_v=0.2c, Γ = 6.7m²/s, and $\overline{\Gamma}$ = 1.214. It is evident in Fig. 6 that the third quadrant BVI data again differs subtly from the parallel BVI data, and in different ways than evidenced by the second quadrant oblique BVI data of Fig. 5. In the C_n history of Fig. 6, it is apparent that unlike in Fig. 5, here the C_n values from the oblique BVI start out lower than the than C_n values of the parallel case. The oblique case C_n values remain lower throughout the approach of the interaction vortex, reach a lower but comparably peaked maximum, and then plunge steeply towards the minimum in a manner similar to that of the parallel C_n values. Subsequent to the main C_n plunge, both curves show similarly scaled trailing edge moment perturbations, offset by a small phase shift. Following this the two curves converge back on zero. The C_m curves are qualitatively similar to each other, apart from the previously mentioned small phase shift. The C_t curves reveal larger peaks in the parallel data, in addition to the same small phase shift.

Except for the slight phase shift, the comparison of data in Fig. 6 is typical of third quadrant to parallel BVI

comparisons, although in some cases the moment data reveals differences in peak magnitudes. The behaviour of the normal and tangential forces during the approach of the interaction vortex is particularly representative of such comparisons.

Discussion

The pressure measurements taken during the oblique blade-vortex interactions examined in this study showed many similarities to data collected during parallel blade-vortex interactions. Features of the unsteady pressure distribution about the aerofoil were found similar in their effect upon the integrated force and moment coefficients for both parallel and oblique interactions. The magnitudes of normal and tangential force coefficients were found to correspond to the nondimensional vortex strength. Alterations in the form of C_m histories were found to change with vortex height in a manner similar to that observed for parallel interactions by Horner et al[17]. Variations in blade-vortex intersection angle were found to effect C_n and C_t data differently depending upon the quadrant of the interaction.

The powerful effect of the nondimensional vortex strength in controlling C_n magnitudes is examined in Fig. 7. The maximum C_n attained in test cases using the strongest vortex ($\Gamma = 6.7$ m^2/s), and with the vortex height (Y_v) set at 0.2c, is plotted against nondimensional vortex strength, and implicitly in the nondimensionalisation of $\bar{\Gamma}$, Z_v. The symbols representing data points are grouped by span location. Also superimposed upon the plot is a line fit to the data points from each span location. It is apparent that at each span location the value of the peak C_n attained is dependent on the nondimensional vortex strength. It is also apparent that the rate of increase in C_n maximum, with respect to $\bar{\Gamma}$, is greatest at inboard locations, and is slightly lower at each consecutive outboard measurement location. This decline in C_n maximum at outboard locations may be associated with the finite span of the rotor blade producing tip flows which suppress normal forces at outboard locations.

Although the magnitudes of minimum C_t values increase with $\bar{\Gamma}$, it is not clear whether this is a linear or quadratic relationship. A scatter plot presenting the values of the C_t minima across a range of $\bar{\Gamma}$ are presented in Fig. 8. Data are grouped by span position, and as in Fig. 7, they represent a variety of Z_v values, but were all measured with $Y_v = 0.2$c, and $\Gamma = 6.7$ m^2/s.
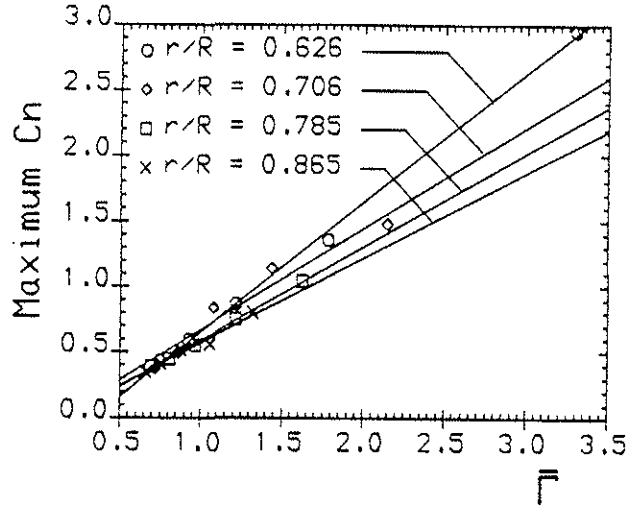
Fig. 7: A plot of the maximum C_n obtained vs. nondimensional vortex strength. Data are grouped by span location, and reflect $Z_v/c = 2, 1, 0, -1, -2$. $Y_v/c = 0.2$ in all cases.
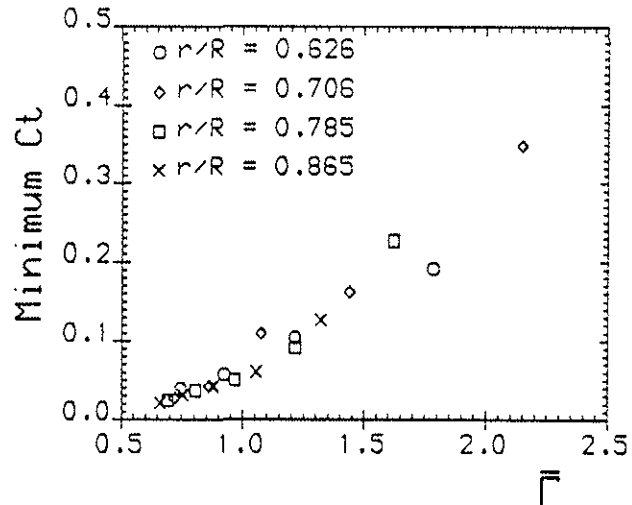
Fig. 8: A plot of the minimum C_t obtained vs. nondimensional vortex strength. Data are grouped by span location, and reflect $Z_v/c = 2, 1, 0, -1, -2$. $Y_v/c = 0.2$ in all cases.

Although the magnitudes and other gross features of the oblique BVI data are in many ways governed by parameters present during parallel interactions, the effect of Z_v, the parameter controlling the blade-vortex intersection angle, is also evident in this study.

During second quadrant oblique blade-vortex interactions, the initial C_n values were greater than in corresponding parallel cases. As the vortex further approached, the
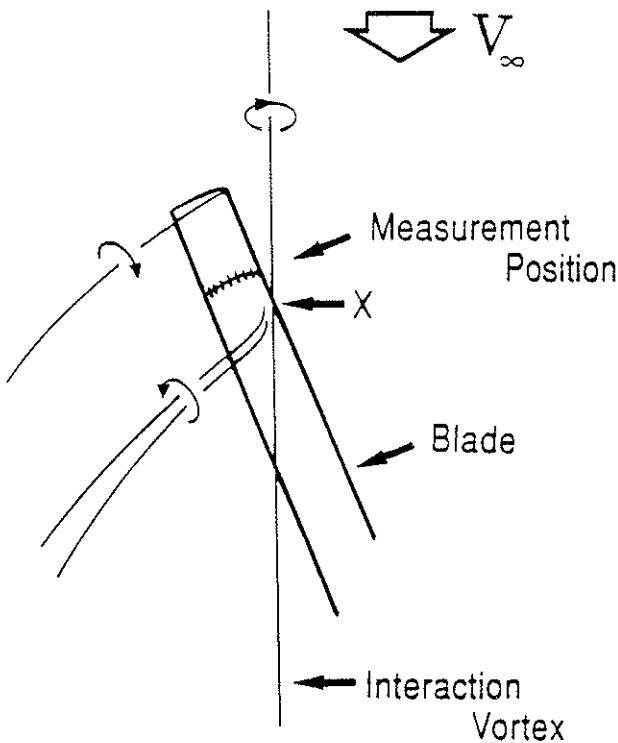
Fig. 9: Caricature of a second quadrant BVI.

oblique C_n data were surpassed by the parallel C_n data, which reached a higher and sharper peak, and then dropped more abruptly towards the C_n minimum value. Data collected after the vortex passed the aerofoil leading edge showed greater similarity between the oblique and parallel C_n assessments. An explanation of these trends may be obtained by examining the three-dimensionality underlying the oblique interactions.

A caricature of a second quadrant BVI is depicted in Fig. 9. The blade is advancing in the clockwise sense, interacting with a vortex set to the left (the positive Z_v direction) of the rotor hub and tunnel centreline. The point where the vortex intersects the blade is labelled "X", and it moves outboard as the azimuth advances. From the normal force data it is apparent that lift is generated at span positions outboard of the point "X", while negative lift is generated at positions inboard of the point "X". From this it is accepted that the circulation about the aerofoil is positive outboard of "X" and negative inboard of "X". Application of Helmholtz' vortex theorems further suggests that this circulation must extend into the wake of the blade in the form of shed vorticity, predominantly at the blade tip and in the region near the point "X". The sense of the vorticity extending from both of these locations is oriented to reduce the angle of attack of flows impinging upon the

rotor blade at positions outboard of the point "X". Although it is not clear whether the vorticity shed into the wake near the point "X" rolls up into a discrete vortex, for convenience this vorticity will be referred to collectively as the "intersection vortex".

The flow structures postulated in Fig. 9 could account for the observed differences between C_n histories collected under parallel and second quadrant oblique conditions. During the approach of the interaction vortex towards the measurement pod the tip regions of the rotor blade are further from the interaction vortex than the measurement position. This would result in a tip vortex that is weaker at a given value of X_v than under parallel interaction conditions, when the measurement position and the tip are almost equal distances from the interaction vortex. The result would be less reduction in incidence by the tip vortex early in the interaction, and therefore larger C_n values at the beginning of the C_n history, for the oblique condition.

Subsequently, as the vortex draws nearer to the measurement position, the position "X", and the associated "intersection vortex" would move outboard, suppressing incidence increases due to the rapidly approaching interaction vortex. Because of the small magnitudes of the intersection angles, the "intersection vortex" would approach the measurement position faster than the interaction vortex. Only at the very last moment before coincidence of "X" and the measurement station does it draw near enough to significantly reduce the incidence induced by the interaction vortex. The smaller the interaction angle between the blade and the vortex, the quicker would be the approach and the briefer would be the effect of the "intersection vortex". In the parallel BVI geometries utilised in this experiment, the vortex generator was aligned directly upstream of the rotor hub, resulting in a slightly oblique geometry at all but the 180° azimuth position. Thus even in the parallel cases this "intersection vortex" would briefly effect the flows in the measurement position, but for a far shorter portion of the test run. As a result, the C_n data collected during the oblique interaction would reflect a greater reduction of C_n values over slightly more of the cycle immediately preceding the arrival of the interaction vortex at the leading edge of the measurement pod. The rounding of the C_n peak and its early drop towards the negative values would follow.

The C_t histories show a response to second quadrant geometries that is similar to that of the C_n values. The reduced, rounded C_t peaks effected by second quadrant conditions would follow from the same reductions in leading edge incidence and leading edge suction

responsible for the alterations in C_n behaviour. The effect that the three-dimensional flows would exert upon the leading edge would be manifest in both the horizontal and vertical components of the force integrated from the pressure distributions.

Although the C_m histories were less consistent than those of C_n and C_t, the initial C_m peak was generally as large or larger under oblique conditions than under parallel conditions. It is possible that this may reflect a lowering of the height of the interaction vortex, effected by the downwash of the implied "intersection vortex".

During third quadrant blade-vortex interactions the C_n data started with lower values than in corresponding parallel cases. The oblique C_n data curve remained below the parallel curve while both increased at about the same rate towards a peak of a similar shape, both then descended abruptly towards a minimum, again at approximately the same rate.

The geometric conditions underlying third quadrant oblique blade vortex interactions are very different from those underlying second quadrant interactions, and result in substantial differences in the evolution of the three-dimensional flow structures likely to occur during interactions. Fig. 10 presents a schematic of a third quadrant oblique BVI. As in Fig. 9, the blade is advancing in the clockwise direction, but this time the vortex generator is set towards the right (the negative Z_v direction) of the rotor hub and the tunnel centreline. The intersection point, again labelled "X", does not exist until shortly before the vortex reaches the measurement position. The vortex first intersects the rotor tip, and the intersection then moves inboard rapidly. Span positions inboard of "X" produce positive lift, while in outboard positions lift is negative. As before, this spanwise variation in lift suggests a tip vortex that suppresses incidence at inboard locations until the intersection has begun at the tip. Here a new tip vortex develops having the opposite sense, i.e. increasing the incidence of inboard locations, while at the same time the original tip vortex is strengthened and effectively becomes the new "intersection vortex". This "intersection vortex" has the same effect as under second quadrant conditions, again reducing the incidence at the measurement location, but this time it is moving inboard from the tip as the azimuth progresses.

The effect of this flow development is again seen most clearly in the C_n history. The initial C_n values obtained under third quadrant oblique conditions are less than those observed under parallel conditions. This again reflects the increased influence of the tip vortex in the case where
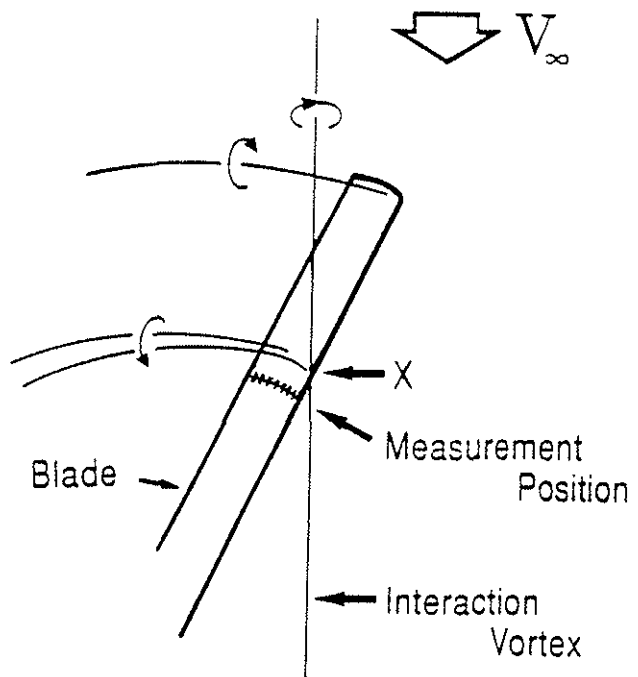

Fig. 10:   Caricature of a third quadrant BVI.

the tip is closer to the vortex at a given X_v/c. In the comparison of second quadrant oblique to parallel conditions, it was the parallel case that was thus reduced. In the comparison between third quadrant oblique and parallel interactions, however, it is the third quadrant oblique interaction that gets the early reduction in incidence and the corresponding reduction in the early C_n values.

After the rotor tip meets the interaction vortex, the flows at the measurement position receive an increase in incidence from the tip vortex, and a growing reduction in incidence with the approach of the "intersection vortex. Thus although the measurement position continues to be influenced by stronger reductions in incidence than under parallel conditions, the extra reduction associated with the approach of the "intersection vortex" is partially cancelled by the upwash of the tip vortex. The result is that the C_n values reach a peak of much the same shape, if of lower magnitude, than under parallel conditions.

The effect of the tip vortex is particularly influential in the comparisons between third quadrant oblique and parallel interactions made in this study. Because the oblique tests were only run with the strongest vortex ($\Gamma = 6.7$ m^2/s), the only way to increase the third quadrant nondimensional vortex strengths was to use further outboard measurement locations for the third quadrant interactions. The use of these outboard locations

491

compensates for the reduction in relative wind inherent in the third quadrant by substituting the increase in relative wind inherent at outboard locations. Although the use of these different span locations does result in a more *appropriate scaling of the interactions compared, it also* results in a greater influence of tip flows in the third quadrant oblique case.

Conclusion

The pressure histories measured about the test aerofoil during the blade-vortex interactions examined in this study revealed many qualitative and quantitative similarities between data collected during parallel and oblique interactions. The rise and collapse of the leading edge suction peak appeared similar under parallel and oblique conditions, as did the convective disturbances associated with the close overhead passage of the interaction vortex.

The force and moment data integrated from the pressure histories also maintained the same gross features under parallel and oblique conditions.

The magnitudes of the peaks, valleys and perturbations of all data were strongly dependent upon the nondimensional vortex strength used during test runs. This appeared particularly true for normal force data, were a strong linear relation between C_n maximum and $\bar{\Gamma}$ was noted.

Differences between data collected under parallel and oblique conditions were observed. While these differences were of a smaller magnitude than some of the differences resulting from other parameter variations, they served to highlight the three-dimensional nature of the flows generated during blade vortex interactions. These flows yielded largely different effects depending upon whether tests were conducted in the second or the third azimuthal quadrant. This suggests that in full rotor tests similar variations in flow structure might arise depending upon whether interacting vortices were inclined towards the root or the tip of the rotor blade.

Acknowledgements

References

1.   Scheiman, J. and Ludi, L.H., "Qualitative Evaluation of Effect of Helicopter Rotor-Blade Tip Vortex on Blade Airloads"NASA TN D-1637, May, 1963.

2.   Surendraiah, M. "An Experimental Study of Rotor Blade-Vortex Interaction", M.S. Thesis. The Pennsylvania State University, December. 1969.

3.   Padakannaya, R. "Experimental Study of Rotor Unsteady Airloads due to Blade Vortex Interaction", NASA CR - 1909, November, 1971.

4.   Caradonna, F.X., Laub, G.H. and Tung, C. "An Experimental Study of Rotor-Vortex Interaction", NASA TM-86005, November, 1984.

5.   Caradonna, F.X., Lautenschlager, J.L. and Silva, M.J., "An Experimental Study of Rotor-Vortex Interactions", AIAA Paper 88-0045, AIAA 26th Aerospace Sciences Meeting, Reno, Nevada, January, 1988.

6.   Ham, N.D. "Some Preliminary Results from an Investigation of Blade-Vortex Interactions", Journal of the American Helicopter Society, Vol. 19, pp. 45-48, April, 1974.

7.   Ham, N.D. "Some Conclusions from an Investigation on Blade-Vortex Interaction", Journal of the American Helicopter Society, Vol. 20, pp 26-31. October, 1975.

8.   Seath, D.D. "Vortex-Airfoil Interaction Tests", 2nd Atmospheric Flight Mechanics Conference, Palo Alto and Moffet Field, California, September, 1972.

9.   Seath, D.D., Kim, J.M. and Wilson, D.R. "An investigation of the Parallel Blade-Vortex Interaction in Low-Speed Wind Tunnel", AIAA Paper 87-1345, AIAA 19th Fluid Dynamics, Plasma Dynamics and Lasers Conference, Honolulu,Hawaii, June, 1987.

10. Booth, E.R. Jr. and Yu, J.C. "Two-Dimensional Blade-Vortex Flow Visualisation Investigation", AIAA Journal Vol. 24, No. 9, September, 1986.

11. Booth, E.R. Jr.
"Surface pressure Measurement During Low Speed Two-Dimensional Blade Vortex Interaction", AIAA Paper 86-1856, AIAA 10th Aeroacoustics Conference, Seattle, Washington, July, 1986.

12. Meier, G.E.A. and Timm, R.
"Unsteady Vortex Airfoil Interaction"
AGARD CP - 386, May, 1985.

13. Kokkalis, A. and Galbraith, R.A.McD.
"Description of, and Preliminary Results from, a New Blade-Vortex Interaction Test Facility", 12th European Rotorcraft and Powered Lift Aircraft Forum, Garmisch - Partenkirchen, Federal Republic of Germany, September, 1986.

14. Kokkalis, A. and Galbraith, R.A.McD.
"Results from the Glasgow University Blade-Vortex Interaction Facility", 13th European Rotorcraft and Powered Lift Aircraft Forum, Arles, France, September, 1987.

15. Straus, J., Renzoni, O. and Mayle, R.E.
"Airfoil Pressure Measurements During a Blade-Vortex Interaction and a Comparison with Theory",AIAA Paper 88-0669, AIAA 26th Aerospace Sciences Meeting, Reno, Nevada, January, 1988.

16. Horner, M.H., Saliveros, E., Kokkalis, A., and Galbraith, R.A.McD., "Results from a Set of Low Speed Blade-Vortex Interaction Experiments", Glasgow University Aero Report 9109, July, 1991.
To Be Published Externally.

17. Horner, M.H., Saliveros, E., and Galbraith, R.A.McD., "An Examination of Vortex Convection Effects During Blade-Vortex Interaction", American Helicopter Society International Technical Specialists Meeting/Rotorcraft Acoustics and Rotor Fluid Dynamics, Oct. 1991.

18. Sears, W.R.
"Aerodynamics, Noise and the Sonic Boom", AIAA Journal, Vol. 7, No. 4, April, 1969.

19. Panaras, A.
"Numerical Modelling of the Vortex-Airfoil Interaction", AIAA Journal, Vol. 25, No. 1, January, 1987.

20. Lee, D.J. and Smith, C.A.
"Distortion of Vortex Core During Blade/Vortex Interaction", AIAA Paper 87-1243, AIAA 19th. Fluid Dynamics, Plasma Dynamics & Lasers Conference Honolulu, Hawaii, June, 1987.